Journal of Solid State Chemistry 181 (2008) 1445–1455

Contents lists available at ScienceDirect

Journal of Solid State Chemistry

journal homepage: www.elsevier.com/locate/jssc

Structural characterisation of the $Ce_{1-x}La_xNbO_{4+\delta}$ solid solution series: *In-situ* high-temperature powder diffraction studies

R.J. Packer, P.A. Stuart, S.J. Skinner *

Department of Materials, Imperial College London, Prince Consort Road, London SW7 2BP, UK

ARTICLE INFO

Article history:
Received 28 January 2008
Received in revised form
13 March 2008
Accepted 22 March 2008
Available online 27 March 2008

Keywords:
Cerium niobate
Neutron diffraction
X-ray diffraction
Lanthanum substitution
Phase diagram and scheelite

ABSTRACT

High-resolution neutron powder diffraction has been utilised to investigate the effect of lanthanum substitution on the structure of cerium niobate, $CeNbO_{4+\delta}$, as a function of temperature. Two members of the $Ce_{1-x}La_xNbO_{4+\delta}$ solid solution series, $Ce_{0.8}La_{0.2}NbO_{4+\delta}$ and $Ce_{0.2}La_{0.8}NbO_{4+\delta}$, were examined over a temperature range of 293–923 K under a positive pressure of O_2 (500 mbar). From this data it was found that on increasing lanthanum substitution there was an associated reduction in the temperature of the monoclinic-to-tetragonal phase transition. The data also suggested that increasing lanthanum substitution caused an associated decrease in the excess oxygen content. In addition, high-temperature X-ray powder diffraction data recorded in static air were also examined for four compositions of the $Ce_{1-x}La_xNbO_{4+\delta}$ series ($x = 0.2$, 0.4, 0.6 and 0.8). These data corroborated the results of the neutron diffraction experiments and also suggested that there was formation of an intermediate phase, analogous to the $CeNbO_{4.08}$ phase of the parent material, during the phase transitions of the $x = 0.8$ and 0.6 compositions.

1. Introduction

The drive for new energy production techniques and technologies is currently of great interest primarily because of concerns over the sustainability of fossil fuels and the effect their emissions have on the environment. As such solid oxide fuels cells (SOFCs) are being extensively researched [1] due to their high efficiencies, flexible fueling choices and lower emissions. The challenge of increasing power output of SOFCs at lower operating temperatures is dependant on several factors including cathode performance and charge transfer kinetics which are affected by the rate of oxide ion diffusion through the materials used in their design and construction. Hence ceramics exhibiting high oxide ion mobility are of great importance.

In the past the main focus of research has been on materials that contain lattice vacancies through which oxide ion conduction is achieved, with fluorite-structured yttria stabilised zirconia (YSZ) and gadolinium-doped ceria (CGO) being typical electrolyte materials and perovskite structured materials such as $La_{1-x}Sr_xMnO_{3-\delta}$ (LSM) and $La_{1-x}Sr_xCo_{1-y}Fe_yO_{3-\delta}$ (LSCF) chosen as the cathodes [2]. More recently it has been shown that interstitial oxygen-containing materials can also possess high oxygen mobility. One such example is that of the K_2NiF_4-type oxide, lanthanum nickelate, $La_2NiO_{4+\delta}$, which has an oxide ion tracer diffusion coefficient of $1.73 \times 10^{-7}\,cm^2\,s^{-1}$ at 1073 K [3] and has shown promise as a possible SOFC cathode component [4]. Viable materials showing significant interstitial oxide ion conduction are limited, but one interesting possibility is the orthoniobate, $CeNbO_{4+\delta}$.

Cerium niobate, $CeNbO_{4+\delta}$, has a room temperature monoclinic fergusonite structure [5] and is particularly interesting due to its wide range of oxygen stoichiometries varying from stoichiometric $CeNbO_4$ to $CeNbO_{4.33}$ [6]. In this range there are four distinct structure types that can be identified and attributed to stoichiometries of $CeNbO_4$, $CeNbO_{4.08}$, $CeNbO_{4.25}$ and $CeNbO_{4.33}$. The oxygen excess is believed to be incorporated on interstitial sites and the charge balanced by the oxidation of Ce^{3+} to Ce^{4+}. Another interesting feature of $CeNbO_{4+\delta}$ is that it exhibits a phase change at approximately 1023 K in air to a tetragonal scheelite structure [7].

Recent studies of the electrical properties of cerium niobate showed the material to have a reasonably high total conductivity ($0.030\,S\,cm^{-1}$ at 1123 K); however, it revealed the ionic transference number to be 0.4 (mixed ionic/p-type electronic conductor) [8]. This study also identified the high-temperature polymorph (scheelite tetragonal) to be unstable at low partial oxygen pressures. Encouragingly further work established that the oxide ion diffusion in the material was relatively high ($D^* = 8.29 \times 10^{-8}\,cm^2\,s^{-1}$ at 1123 K) along with a good surface exchange coefficient ($k^* = 6.85 \times 10^{-7}\,cm\,s^{-1}$ at 1123 K) [9]. This research

* Corresponding author. Fax: +44 20 7594 6757.
E-mail address: s.skinner@imperial.ac.uk (S.J. Skinner).

0022-4596/$ - see front matter © 2008 Elsevier Inc. All rights reserved.
doi:10.1016/j.jssc.2008.03.016

also established enhanced oxide ion tracer diffusion coefficients in the low-temperature monoclinic fergusonite structure.

These results indicated that, although the material showed many promising attributes for use as an SOFC component material, optimisation would be required to enhance the conduction properties before applications could be considered. This was attempted via lanthanum substitution on the *a* (cerium) site. The selection of La as a substituent was the result of the similar ionic radii of cerium and lanthanum and the stable oxidation state of the La species (La^{3+}). It was envisaged that this would increase the ionic transference number, possibly leading to SOFC electrolyte applications, and stabilise the structure at low partial oxygen pressures. It was also foreseen that this would lower the transition temperature to the scheelite structure as the transition temperature in $LaNbO_4$ was reported to be 793 K [10]. EMF measurements confirmed the increase in transport number and are presented elsewhere [11]; however, further *in-situ* structural characterisation of the lanthanum-substituted ceramics with temperature was required to establish the stability of the materials and are the focus of the current work.

2. Experimental

Samples of the general formula $Ce_{1-x}La_xNbO_{4+\delta}$ ($x = 0$, 0.2, 0.4, 0.6, 0.8 and 1) were prepared following the method employed by Thompson et al [6]. The dried component oxides, CeO_2 (Aldrich, 99.9%), La_2O_3 (Aldrich, 99.9%) and Nb_2O_5 (Aldrich, 99.99%) were mixed together, in stoichiometric amounts, in a mortar and pestle under acetone to ensure a homogeneous mixture was achieved. The mixtures were subsequently heated (600 K h^{-1}) in air in alumina crucibles to 1273 K for a period of 12 h, cooled (300 K h^{-1}) and ball milled (48 h). The milled material was then heated (600 K h^{-1}) for a further 18 h at 1673 K before being quenched rapidly in air.

Phase purity was confirmed using a Philips PW1700 series powder X-ray diffractometer with Cu-$K\alpha$ radiation ($\lambda = 1.5418$ Å) and a graphite secondary crystal monochromator. Oxygen stoichiometry was determined from thermogravimetric analysis in flowing air using a Netzsch STA 449C Jupiter simultaneous TG-DTA/DSC instrument in the temperature range of 298–1273 K with a heating/cooling rate of 10 K min^{-1} and is fully reported elsewhere [11].

Neutron powder diffraction data were collected from 3 g samples contained in quartz sample tubes under a positive oxygen partial pressure of 500 mbar on the HRPD diffractometer using both 90° and backscattering detectors at ISIS, Rutherford Appleton Laboratory, Oxfordshire, UK. Each data set was recorded for circa. 120 mins and then normalised and corrected in the usual way. Data was analysed by Rietveld refinement using the GSAS/EXPGUI programme [12,13].

In-situ high-temperature X-ray diffraction (HT-XRD) studies were performed on a PANalytical X'pert diffractometer with a Bühler HDK 2.4 temperature stage with a Pt heating strip. Once again Cu-$K\alpha$ radiation with a graphite secondary crystal monochromator was used. Data were collected over the temperature range 308–1123K with measurements on both heating and cooling. Heating and cooling rates were 60 K min^{-1} with a 1 min dwell time prior to data collection for 2 h duration. Calibration of the temperature of the sample was achieved using temperature sensitive thermal paint.

3. Results

3.1. $Ce_{0.2}La_{0.8}NbO_{4+\delta}$

The room temperature neutron powder diffraction data (under a positive pressure of O_2) for the $Ce_{0.2}La_{0.8}NbO_{4+\delta}$ material were fitted to the parent $CeNbO_4$ [14] low-temperature monoclinic fergusonite structure ($I2/a$) (Fig. 1(a)) and provided a good fit with a low χ^2 value of 1.170, $R_p = 5.54\%$ and $R_{wp} = 6.37\%$.

Refinement of the room temperature unit cell gave lattice parameters of 5.19470(5) Å, 11.50069(11) Å and 5.56301(6) Å for *a*, *b* and *c*, respectively with a β angle of 94.222(1)° and a unit cell volume of 331.447(8) $Å^3$. These parameters are, as expected, smaller than those of the end member $LaNbO_4$ due to the smaller ionic radii of Ce^{3+} when compared with La^{3+} ($LaNbO_4$, $a = 5.2042(8)$ Å, $b = 11.5206(39)$ Å, $c = 5.5682(9)$ Å, $\beta = 94.09(1)°$ and $V = 332.99$ $Å^3$ [15]). Whilst the *a*, *b* and *c* lattice parameters for the $Ce_{0.2}La_{0.8}NbO_{4+\delta}$ sample were smaller than those of $LaNbO_4$, the β angle is slightly larger in the $Ce_{0.2}La_{0.8}NbO_{4+d}$ substituted sample. On examining the literature it is clear that the β angle for the end member $CeNbO_4$ is significantly larger than that for the $LaNbO_4$ and that the angle reported here fits the previously reported data well, with $LaNbO_4$ having the smallest room temperature β angle of the lanthanide orthoniobates including $CeNbO_4$ [5].

Table 1 shows the refined atomic positions of the room temperature $Ce_{0.2}La_{0.8}NbO_{4+\delta}$ and indicates very little deviation in the oxygen positions from that of the parent material, suggesting minimal interstitial oxygen content. The *a* site occupancies showed minor deviations from the 0.8/0.2 nominal

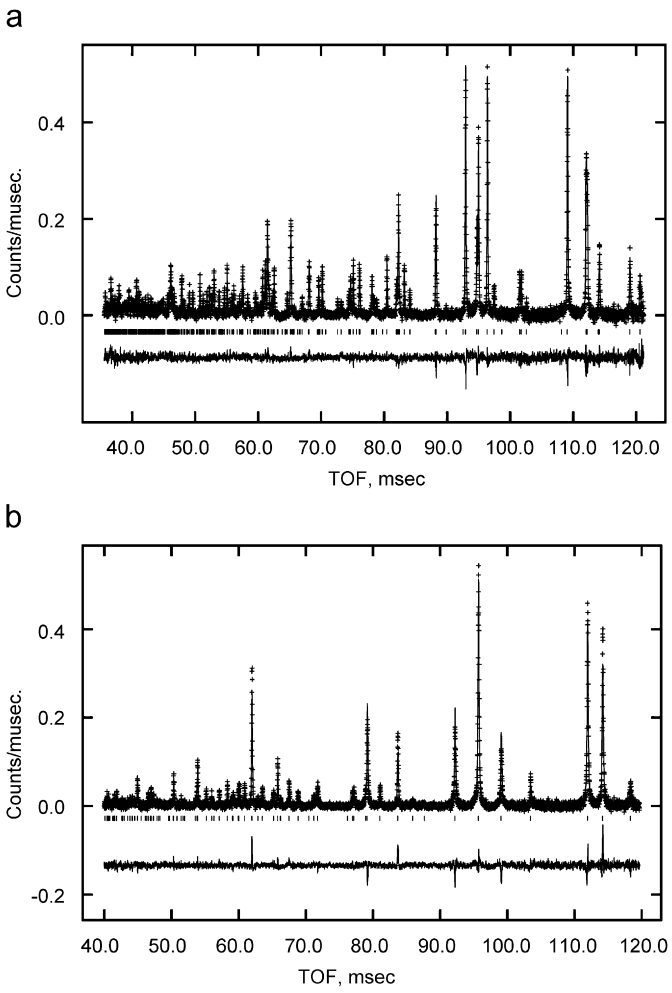

Fig. 1. Rietveld refinement difference plots obtained from powder neutron diffraction data for $Ce_{0.2}La_{0.8}NbO_{4+\delta}$ under 500 mbar positive pressure of O_2 (a) at room temperature (monoclinic $I2/a$) and (b) 873 K (tetragonal $I4_1/a$). The experimental and calculated profiles are represented by crosses and a full line, respectively. The difference plot is below with tick marks indicating the positions of the Bragg reflections.

composition; however, the refined site occupation is within the refinement error. It is interesting to note that oxygen deficiencies are witnessed and these may be accommodated on the interstitial sites (Frenkel defects); however, refining the proposed interstitial positions proved difficult. The temperature factors of the metal atoms were fixed on refinement to a slight positive value; however, the oxygen positions were refined and are seen to exhibit some anisotropy.

Between 773 and 823 K a transition to a tetragonal scheelite structure occurred as witnessed previously in the parent cerium and lanthanum orthoniobates. The temperature at which this occurred agreed well with the observation that the ionic radii of a rare earth affects the temperature of the transition with the largest lanthanide (lanthanum) exhibiting the lowest transition temperature [16]. The high-temperature diffraction data were fitted to the structure of the tetragonal scheelite $CeNbO_4$ [7] (Fig. 1(b)) and once again gave a good fit, in this case with a χ^2 value of 1.394, $R_p = 6.15\%$ and $R_{wp} = 7.20\%$.

Refinement of the 873K unit cell gave lattice parameters of $a = b = 5.40046(3)$ and $c = 11.66892(10)$ Å with a unit cell volume of 340.324(4) Å^3. Results of the refinement of the atomic positions are given in Table 2. The occupancies of all the cation sites were fixed to the ratio observed at room temperature. The oxygen positions were allowed to fluctuate but showed little deviation from the oxygen position in $CeNbO_4$ ($x = 0.1650(20)$, $y = 0.4947(20)$ and $z = 0.21151(75)$) [15]. Once again it is interesting to note that the occupancy of the oxygen position appears slightly deficient, which maybe due to Frenkel defects, but in this instance the difference is small with the values within the error of the refinement.

On heating $Ce_{0.2}La_{0.8}NbO_{4+\delta}$ the variation in lattice parameter with increasing temperature (Table 3) is reasonably uniform. The a and c parameters (Fig. 2(a)) are seen to converge (as the convergence is gradual it indicates minimal oxidation). Due to this convergence the overall volume becomes dependant on the b parameter and this can be seen from Figs. 2(b) and (d) which show almost identical patterns. Finally we observe asymptotic reduction in the β angle in the monoclinic phase with temperature (Fig. 2(c)). Note that the greatest errors occur at 773 K and are a result of there being a mixture of two phases present during this transition. This is further highlighted by HT-XRD data and is shown later in this section.

The change in bond length (Table 4) of one of the La(Ce)–O1 bonds follows an expected pattern, increasing linearly with temperature in the monoclinic phase; this is a further indication of the lack of oxidation and interstitial content (the proposed interstitial site [6] being in the La/Ce coordination sphere). This is then followed by a reduction in bond length after the phase transition. This is not the case for the Nb–O1 bond lengths, which do not appear to show a direct pattern. However, the O1–Nb–O1 bond angles follow the same pattern as the La–O1 bond lengths. The significant reduction in O1–Nb–O1 bond angle, 112.02(35)–106.13(7)°, after the phase transition can be attributed to the change in coordination from highly distorted six coordinate in the monoclinic structure to four coordinate in the tetragonal polymorph (Fig. 3).

Finally HT-XRD data presents further evidence for the phase transition occurring between 723 and 823 K. Fig. 4(a) shows the XRD patterns for $Ce_{0.2}La_{0.8}NbO_{4+\delta}$ on heating and clearly shows the change of structure to the tetragonal phase at 806 K. These data also highlight the absence of interstitial oxygen in the monoclinic phase as there are no peaks present between 30° and 35° 2θ. It is this region of the diffraction pattern that is indicative of a $CeNbO_{4.08}$ oxidised phase and between 573 and 873 K there is no significant intensity observed in this region. This indicates that the $Ce_{0.2}La_{0.8}NbO_{4+\delta}$ monoclinic phase does not undergo oxidation at temperatures below 806 K at which point there is a transformation to the tetragonal modification.

As discussed earlier the HT-XRD data suggest that the errors in the neutron data recorded at 773 K arise due to a mixture of the monoclinic and tetragonal phases being present. This is because the 710 K HT-XRD data clearly shows peaks attributable to both the monoclinic and tetragonal phases (Fig. 4(a)). This effect is also observed on cooling from 1096 to 710 K. After cooling to room temperature the XRD pattern is unchanged from that recorded before the heating cycle. This lack of hysteresis is an indication of lack of oxidation as cooling in air results in a change in the powder diffraction pattern of the parent material, $CeNbO_4$, to a pattern reminiscent of the mixed $CeNbO_4$/$CeNbO_{4.08}$ phases. This mixed phase is attributable to oxidation of Ce^{3+} [17]. Clearly this is not observed with the La-substituted material.

Thermogravimetric analysis reported elsewhere [11] confirms both the neutron diffraction and HT-XRD results in that there is minimal oxidation of the monoclinic crystal due to the extremely small weight increase between 573 and 723 K in comparison with the other $Ce_{1-x}La_xNbO_4$ phases. The thermal analysis data also indicates a phase change at approx. 800 K which agrees with both sets of diffraction data.

Table 1
Refined atomic positions for $Ce_{0.2}La_{0.8}NbO_{4+\delta}$ determined from *in-situ* high-temperature neutron diffraction data recorded at room temperature under 500 mbar positive pressure of O_2 as fitted to the low-temperature $CeNbO_4$ structure (space group $I2/a$)

Atom	Wyckoff	x	y	z	Occupancy	U_{iso} (Å^2)
La	4*e*	0.75	0.1298(1)	0.5	0.79(1)	0.0001
Ce	4*e*	0.75	0.1298(1)	0.5	0.21(1)	0.0001
Nb	4*e*	0.25	0.1039(1)	0	1.000(7)	0.0001
O1	8*f*	0.4878(3)	0.2039(1)	0.1457(3)	0.967(4)	See below
O2	8*f*	0.0515(3)	0.0332(1)	0.2384(3)	0.969(4)	See below
Atom	U11 (Å^2)	U22 (Å^2)	U33 (Å^2)	U12 (Å^2)	U13 (Å^2)	U23 (Å^2)
O1	0.0027(7)	−0.0003(8)	0.0008(8)	−0.0002(7)	0.0004(6)	−0.0019(7)
O2	0.0053(9)	0.0010(8)	0.0001(8)	0.0028(7)	0.0080(6)	0.0010(7)

Metal atoms isotropic temperature factors were fixed as small positive values. Unit cell: $a = 5.19470(5)$ Å, $b = 11.50069(11)$ Å, $c = 5.56301(6)$ Å, $\beta = 94.222(1)°$ and $V = 331.447(8)$ Å^3 with $\chi^2 = 1.170$, $R_p = 5.54\%$ and $R_{wp} = 6.37\%$.

Table 2
Refined atomic positions for $Ce_{0.2}La_{0.8}NbO_{4+\delta}$ determined from *in-situ* high-temperature neutron data recorded at 873 K under 500 mbar positive pressure of O_2 as fitted to the high-temperature $CeNbO_4$ structure (space group $I4_1/a$)

Atom	Wyckoff	x	y	z	Occupancy	U_{iso} (Å^2)
Ce	4*b*	0	0.25	0.625	0.21	0.0075(8)
La	4*b*	0	0.25	0.625	0.79	0.0075(8)
Nb	4*a*	0	0.25	0.125	1	0.0089(8)
O	16*f*	0.1578(3)	0.4924(4)	0.2091(2)	0.99(1)	See below
Atom	U11 (Å^2)	U22(Å^2)	U33 (Å^2)	U12 (Å^2)	U13 (Å^2)	U23 (Å^2)
O	0.027(1)	0.028(1)	0.0017(7)	−0.004(2)	0.013(9)	−0.0038(8)

Unit cell: $a = b = 5.40046(3)$ Å, $c = 11.66892(10)$ Å and $V = 340.324(4)$ Å^3 with $\chi^2 = 1.394$, $R_p = 6.15\%$ and $R_{wp} = 7.20\%$.

3.2. $Ce_{0.8}La_{0.2}Nbo_{4+\delta}$

The neutron powder diffraction data recorded at room temperature (under a positive pressure of O_2) for the $Ce_{0.8}La_{0.2}NbO_{4+\delta}$

Table 3
Variation of lattice parameters of $Ce_{0.2}La_{0.8}NbO_{4+\delta}$ as a function of temperature as determined by Rietveld refinement from *in-situ* high-temperature neutron diffraction data

T (°C)	T (K)	a (Å)	b (Å)	c (Å)	β (°)	Volume (Å^3)	Phase
19	292	5.19470(5)	11.50069(11)	5.56301(6)	94.222(1)	331.447(8)	Monoclinic
250	523	5.23742(4)	11.56433(7)	5.53604(4)	93.264(1)	334.759(3)	Monoclinic
400	673	5.28499(4)	11.61380(8)	5.50118(4)	92.276(1)	337.389(3)	Monoclinic
450	723	5.31002(5)	11.63147(9)	5.48021(5)	91.767(1)	338.315(3)	Monoclinic
500	773	5.34468(8)	11.64680(16)	5.44903(8)	91.072(1)	339.134(6)	Monoclinic
550	823	5.39909(5)	5.39909(5)	11.66047(15)	90	339.904(6)	Tetragonal
600	873	5.40046(3)	5.40046(3)	11.66893(10)	90	340.324(4)	Tetragonal

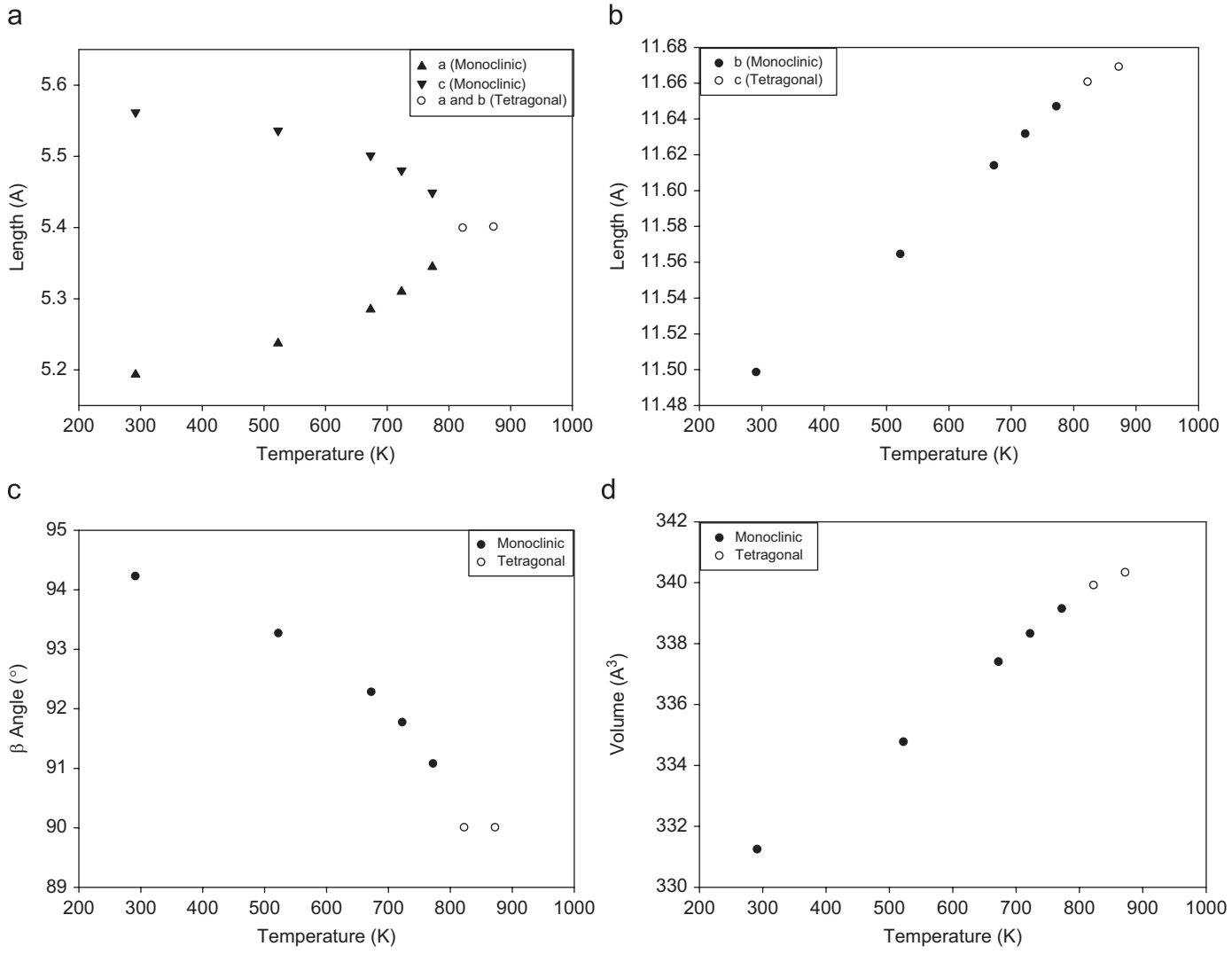

Fig. 2. Variation of (a) a and c lattice parameters, (b) b lattice parameter, (c) β angle and (d) unit cell volume with temperature for $Ce_{0.2}La_{0.8}NbO_{4+\delta}$ refined from *in-situ* high-temperature neutron diffraction.

material were fitted as previously to the parent $CeNbO_4$ low-temperature monoclinic fergusonite structure ($I2/a$) [14]. This refinement once again give a good fit with a χ^2 value of 1.061, $R_p = 5.59\%$ and $R_{wp} = 6.45\%$; however, the signal-to-noise ratio was lower than that of the $Ce_{0.2}La_{0.8}NbO_{4+\delta}$ material. This meant that although the parent cell ($I2/a$) could be fitted reasonably accurately, any expected oxygen excess and subsequent Ce^{3+}/Ce^{4+} long range ordering (as seen in the parent material as extraneous smaller peaks) were not observed.

Refinement of the unit cell gave lattice parameters of $a = 5.5403(2)$ Å, $b = 11.4354(3)$ Å and $c = 5.1744(1)$ Å with a β angle of $94.396(2)^\circ$ and a unit cell volume of $326.86(1)$ Å^3. These data are as expected, with the cell parameters being larger than for the parent material $CeNbO_4$ ($a = 5.5342(2)$ Å, $b = 11.4016(6)$ Å, $c = 5.1583(3)$ Å, $\beta = 94.600(5)^\circ$ and $V = 324.43(2)$ Å^3 [14]) due to the substitution of Ce^{3+} (CN 8, ionic radius of 1.14 Å) with La^{3+} (CN 8, ionic radius 1.16 Å). It should be noted however that in this case the β angle is slightly smaller than the parent $CeNbO_4$ material,

Table 4
Variation of bond lengths and angles with temperature for $Ce_{0.2}La_{0.8}NbO_{4+\delta}$ as determined by Rietveld refinement from *in-situ* high-temperature neutron diffraction data

T (°C)	T (K)	La–O1 (Å)	Nb–O1 (Å)	O1–La–O1 (°)	O1–Nb–O1 (°)
19	292	2.4636(15)	1.8374(17)	139.36(11)	101.95(12)
250	523	2.4786(18)	1.8372(20)	137.98(11)	104.97(14)
400	673	2.4945(20)	1.8451(23)	136.86(12)	107.71(16)
450	723	2.5049(26)	1.8439(29)	136.07(17)	109.98(22)
500	773	2.5090(40)	1.8520(50)	134.70(28)	112.02(35)
550	823	2.5039(20)	1.8454(21)	126.03(7)	106.13(7)
600	873	2.5104(16)	1.8473(17)	125.75(6)	106.43(6)

Lanthanum bond length is for a selected La–O1 bond.

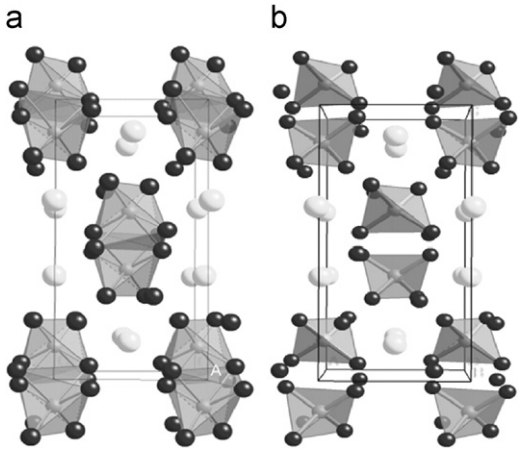

Fig. 3. Representation of the (a) monoclinic and (b) tetragonal structures highlighting the difference in Nb–O coordination environment.

but significantly larger than the end member of the solid solution series, $LaNbO_4$, showing a trend of decreasing angle with increasing La content as observed with the $Ce_{0.2}La_{0.8}NbO_{4+\delta}$ material. Thermogravimetric analysis [11], also suggests a reduction in the interstitial oxygen content when compared to $CeNbO_{4+\delta}$. This in turn suggests a reduction in Ce^{4+}, which has a smaller ionic radius of 0.97 Å, therefore further increasing the size of the unit cell. This conclusion is further supported by HT-XRD data shown in Fig. 5(a) that shows peaks in between the peaks of highest intensity at circa. 29° 2θ that are indicative of the $CeNbO_{4.08}$-related phase in the parent cerium niobate material. Also at 710 K the pattern changes to that of the analogous $CeNbO_{4.25}$ phase seen in the parent material further indicating oxidation.

Table 5 shows the refined atomic positions for the $Ce_{0.8}La_{0.2}NbO_{4+\delta}$ room temperature structure, which correlates well with the $Ce_{0.2}La_{0.8}NbO_{4+\delta}$ material in that there is slight deficiency on the oxygen sites, whilst the cation occupancies remain close to stoichiometry. Whether excess oxygen is found on interstitial sites and if possible long range $Ce^{3+}/La^{3+}/Ce^{4+}$ ordering is present is harder to discern from this data set due to the lower signal-to-noise ratio; however, slight negative values in the temperature factor of the second oxygen position maybe an indicator and as such this was fixed at a low positive number. Once again the Ce/La ratio varies slightly from the nominal stoichiometry proposed but the difference is again within error of the refinement.

The phase change to the tetragonal scheelite structure observed at 823K in the $Ce_{0.2}La_{0.8}NbO_{4+\delta}$ composition was found to occur at 923 K in $Ce_{0.8}La_{0.2}NbO_{4+\delta}$. Increased errors in the refinements of the lattice parameters at 823 K may suggest an intermediate phase is being formed; however, as there are no data for the preceding 200 K it is difficult to comment on this using the neutron diffraction data.

All data recorded above 923 K was refined to the $CeNbO_4$ high-temperature structure, which is tetragonal scheelite, $I4_1/a$ [7]. Once again the χ^2 value, which for the 1023 K data was $\chi^2 = 1.012$ for 40 variables, $R_p = 5.32\%$ and $R_{wp} = 6.27\%$, suggests a very good fit. Refinement of the 1023 K unit cell gave lattice parameters of $a = b = 5.3831(1)$ Å and $c = 11.6114(2)$ Å with a unit cell volume of $336.48(1)$ Å^3. Refinement of the atomic positions (Table 6) were, once again, limited due to all metal ions occurring on fixed Wyckoff sites and as such the occupancies were also fixed to their room temperature-refined values. The oxygen position was refined but showed little deviation from that of $CeNbO_4$ ($x = 0.16181(9)$, $y = 0.49329(12)$ and $z = 0.21018(5)$) [7].

On heating $Ce_{0.8}La_{0.2}NbO_{4+\delta}$ (Table 7) there is a convergence of the a and c parameters (Fig. 6(a)), and a linear expansion in the b parameter (Fig. 6(b)), as observed for the $Ce_{0.2}La_{0.8}NbO_{4+\delta}$ material. The β angle (Fig. 6(c)), and volume (Fig. 6(d)), also mirror the $Ce_{0.2}La_{0.8}NbO_{4+\delta}$ material indicating the major structural changes on heating are essentially unchanged by lanthanum substitution, the only difference being the temperature of the phase change. A minor difference between the two is seen in the a and c parameters, which show a slightly different pattern of convergence to that seen in $Ce_{0.2}La_{0.8}NbO_{4+\delta}$ on heating (Fig. 2(a)). This could suggest that an oxidation process is taking place as an extra oxygen in the cerium coordination sphere coupled with the oxidation of Ce^{3+} to Ce^{4+} would cause changes in the β angle and therefore the a and c parameters.

The changes in bond lengths of $Ce_{0.8}La_{0.2}NbO_{4+\delta}$ (Table 8) are similar to those of the $Ce_{0.2}La_{0.8}NbO_{4+\delta}$ material with the reduction of the Ce–O1 and Nb–O1 bond lengths and the O1–Ce–O1 and O1–Nb–O1 bond angles with the change of phase. There is, however, a slight difference in the 823 and 923 K data. Firstly at 823 K we see a significant increase in the Nb–O1 bond length whereas the previous four temperatures had shown a constant decrease. This maybe due to material gaining extra oxygen that would mean an oxidation of the cerium to Ce^{4+} and a shortening of the Ce–O1 bond and hence a lengthening of the Nb–O1 bonds. This may not be correct, however, as the Ce–O1 bond shows a lengthening and more importantly there is no significant change in the O1–Ce1–O1 bond angle. The other difference is in the 923 K data, which although it fits to a tetragonal pattern shows an unusual pattern in the Ce–O1 bond distance. As expected, the Ce–O1 bond length reduces at the onset of the phase change; however, on further heating it would be expected that the bond length would increase with temperature in the tetragonal phase; however this is not the case. This could be an indication that the material is not fully single-phase tetragonal at this temperature.

The HT-XRD data for the $Ce_{0.8}La_{0.2}NbO_{4+\delta}$ material (Fig. 5(a)), confirms that the phase change occurs at a higher temperature than in the $Ce_{0.2}La_{0.8}NbO_{4+\delta}$ material. There is, however, a slight discrepancy with the neutron data as the phase change was witnessed at the higher temperature of 999 K. This discrepancy could be attributed to a number of different factors, the first of which could be the difference in atmosphere, which in the HT-XRD is static air whereas the neutron work was carried out at 500 mbar positive pressure of O_2. The second reason maybe due to the amount of sample as the HT-XRD required milligrams whereas the neutron data collection required over 3 g. This could result in differences in the thermal equilibration of the samples and hence may result in slight discrepancies in the measured temperature of the samples.

At 903 and 951 K there is evidence of a transitional state before the phase change. The diffraction pattern is consistent with that of the $CeNbO_{4.08}$ phase observed in the parent oxide, cerium niobate. The data also indicates oxidation at lower temperatures. This is

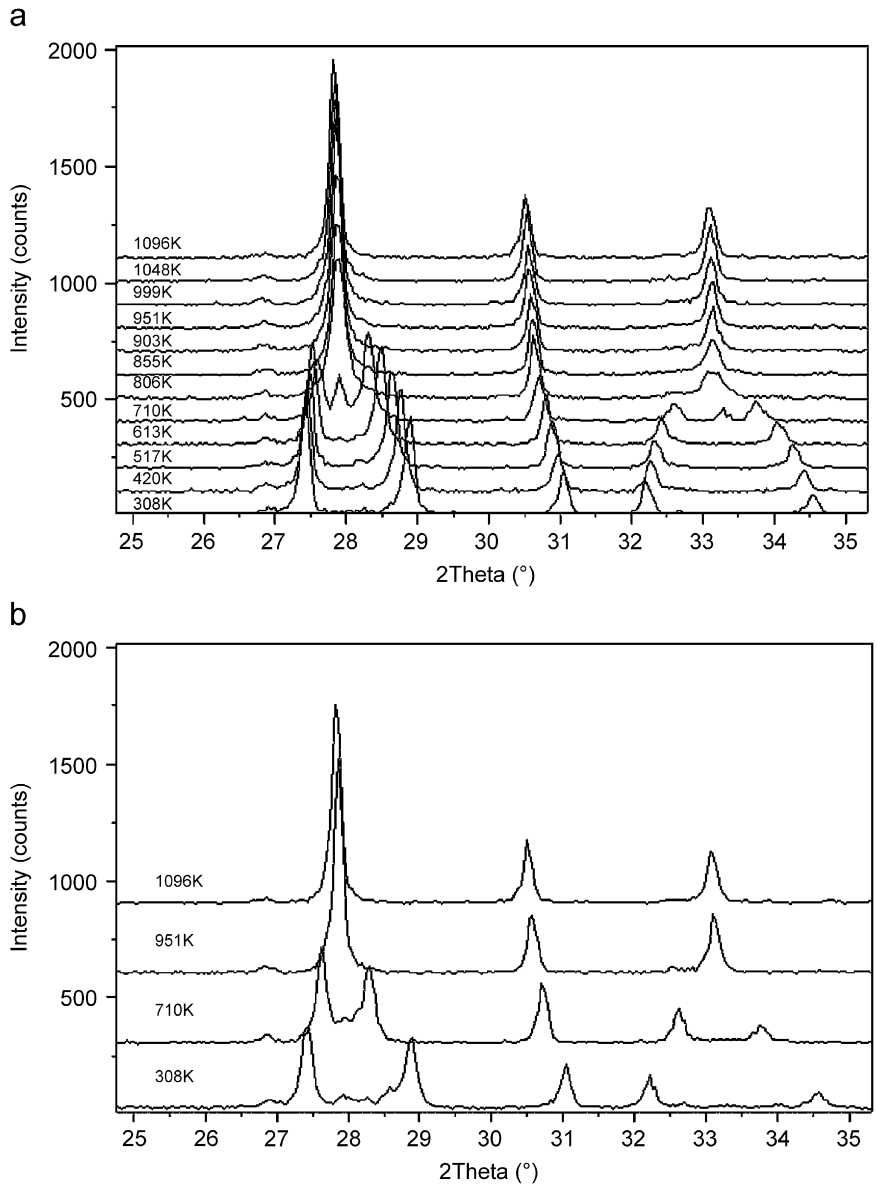

Fig. 4. High-temperature XRD patterns for $Ce_{0.2}La_{0.8}NbO_{4+\delta}$ in static air: (a) pattern obtained between 25° and 35° 2θ on heating and (b) pattern obtained between 25° and 35° 2θ on cooling.

because the room temperature pattern shows smaller peaks in between the peaks of highest intensity at around 30° 2θ which is indicative of the $CeNbO_{4.08}$ related phase in the parent material. Also at 710 K the pattern changes to that of the analogous $CeNbO_{4.25}$ phase in the parent material also indicating significant oxygen excess.

The results are given further credence by TGA data reported elsewhere [11] which indicate an onset of weight change at around 573 K increasing until 823 K and then reducing back to the original weight at 973 K at the point of the phase change. If this weight change is attributed solely to oxygen this would give a material of composition approximately $Ce_{0.8}La_{0.2}NbO_{4.2}$ which corroborates the X-ray data reasonably accurately as the material may have begun with a small amount of oxygen excess at room temperature.

From HT-XRD data on cooling (Fig. 5(b)), we observe a difference from the $Ce_{0.2}La_{0.8}NbO_{4+\delta}$ material in that after a thermal cycle the original room temperature pattern is not replicated. This hysteresis is due to oxidation on cooling in air as the room temperature pattern is consistent with that of the $CeNbO_{4.08}$ hyperstoichiometric phase indicating that on cooling in air the material only partially oxidises. This is because when fully oxidised the material would give a pattern seen in Fig. 5(a) at 710 K, which is analogous to the $CeNbO_{4.25}$ phase in cerium niobate.

3.3. $Ce_{0.6}La_{0.4}Nbo_{4+\delta}$ and $Ce_{0.4}La_{0.6}NbO_{4+\delta}$

HT-XRD was carried out on the $Ce_{0.6}La_{0.4}NbO_{4+\delta}$ and $Ce_{0.4}La_{0.6}NbO_{4+\delta}$ phases in static air and the results are shown in Fig. 7. On heating $Ce_{0.6}La_{0.4}NbO_{4+\delta}$ (Fig. 7(a)), the patterns produced are similar to those of the $Ce_{0.8}La_{0.2}NbO_{4+\delta}$ material in that they show a change of phase (although at the lower temperature of 951 K, as expected) and that a transitional phase similar to the $CeNbO_{4.08}$ phase of the parent material appears to occur before the transition. It is also clear that at 613 K the material oxidises to a phase similar to that of the parent $CeNbO_{4.08}$ and then further

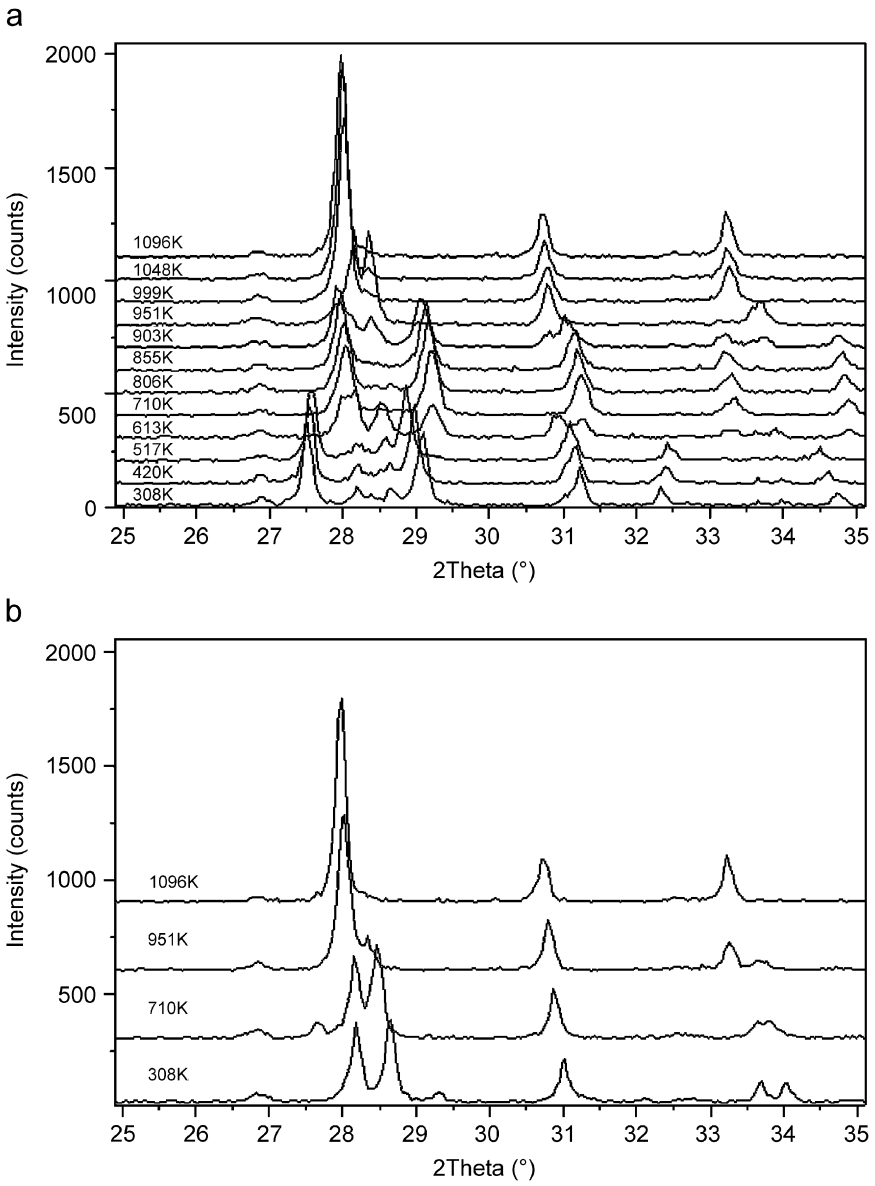

Fig. 5. High-temperature XRD patterns for $Ce_{0.8}La_{0.2}NbO_{4+\delta}$ in static air: (a) pattern obtained between 25° and 35° 2θ on heating and (b) pattern obtained between 25° and 35° 2θ on cooling.

Table 5
Refined atomic positions for $Ce_{0.8}La_{0.2}NbO_{4+\delta}$ as determined from *in-situ* high-temperature neutron diffraction data at room temperature under 500 mbar positive pressure of O_2 as fitted to the low-temperature $CeNbO_4$ structure (space group $I2/a$)

Atom	Wyckoff	x	y	z	Occupancy	U_{iso} (Å2)
Ce	4*e*	0.25	0.1197(6)	0	0.77(6)	0.004(4)
La	4*e*	0.25	0.1199(6)	0	0.23(3)	0.004(2)
Nb	4*e*	0.25	0.6464(5)	0	1.00(1)	0.0001
O1	8*f*	0.0088(9)	0.7192(4)	0.1985(9)	0.92(2)	See below
O2	8*f*	0.8947(8)	0.4540(5)	0.2371(9)	0.99(1)	0.0001
Atom	U11 (Å2)	U22 (Å2)	U33 (Å2)	U12 (Å2)	U13 (Å2)	U23 (Å2)
O1	−0.008(3)	−0.005(3)	0.005(4)	0.011(3)	0.010(2)	0.002(3)

Isotropic temperature factors for niobium and oxygen were fixed at a small positive value. Unit cell: $a = 5.5403(2)$ Å, $b = 11.4354(3)$ Å, $c = 5.1744(1)$ Å, $\beta = 94.396(2)°$ and $V = 326.86(1)$ Å^3 with $\chi^2 = 1.061$, $R_p = 5.59\%$ and $R_{wp} = 6.45\%$.

Table 6
Refined atomic positions $Ce_{0.2}La_{0.8}NbO_{4+\delta}$ as determined from *in-situ* high-temperature neutron diffraction data recorded at 1023 K under 500 mbar positive pressure of O_2 as fitted to the high temperature $CeNbO_4$ structure (space group $I4_1/a$)

Atom	Wyckoff	x	y	z	Occupancy	U_{iso} (Å^2)
Ce	4*b*	0	0.25	0.625	0.78	0.022(2)
La	4*b*	0	0.25	0.625	0.22	0.022(2)
Nb	4*a*	0	0.25	0.125	1	0.013(2)
O	16*f*	0.1606(5)	0.4968(8)	0.2101(3)	0.98(2)	See below
Atom	U11 (Å^2)	U22 (Å^2)	U33 (Å^2)	U12 (Å^2)	U13 (Å^2)	U23 (Å^2)
O	0.033(2)	0.035(2)	0.019(2)	0.009(5)	0.011(2)	−0.003(2)

Unit cell: $a = b = 5.3831(1)$ Å, $c = 11.6114(2)$ Å and $V = 336.48(1)$ Å^3 with $\chi^2 = 1.012$, $R_p = 5.32\%$ and $R_{wp} = 6.27\%$.

Table 7
Variation of lattice parameters with temperature for $Ce_{0.8}La_{0.2}NbO_{4+\delta}$ as refined from *in-situ* high-temperature neutron diffraction data

T (°C)	T (K)	a (Å)	b (Å)	c (Å)	β (°)	Volume (Å^3)	Phase
58	331	5.5403(2)	11.4354(3)	5.1744(1)	94.396(2)	326.86(1)	Monoclinic
250	523	5.5216(1)	11.4858(3)	5.2097(1)	93.642(2)	329.73(1)	Monoclinic
300	573	5.5151(1)	11.4976(3)	5.2193(1)	93.412(2)	330.37(1)	Monoclinic
350	623	5.5075(2)	11.5132(3)	5.2309(2)	93.161(2)	331.18(1)	Monoclinic
550	823	5.4473(3)	11.5731(5)	5.3049(3)	91.547(4)	334.31(2)	Monoclinic
650	923	5.3797(1)	5.3797(1)	11.5944(3)	90	335.56(1)	Tetragonal
700	973	5.3813(1)	5.3813(1)	11.6024(2)	90	335.98(1)	Tetragonal
750	1023	5.3831(1)	5.3831(1)	11.6114(2)	90	336.48(1)	Tetragonal
700	973	5.3813(1)	5.3813(1)	11.6023(2)	90	335.99(1)	Tetragonal
550	823	5.4449(4)	11.5705(8)	5.3095(4)	91.453(5)	334.39(3)	Monoclinic
450	723	4.4860(5)	11.5463(9)	5.2637(5)	92.419(7)	333.12(3)	Monoclinic

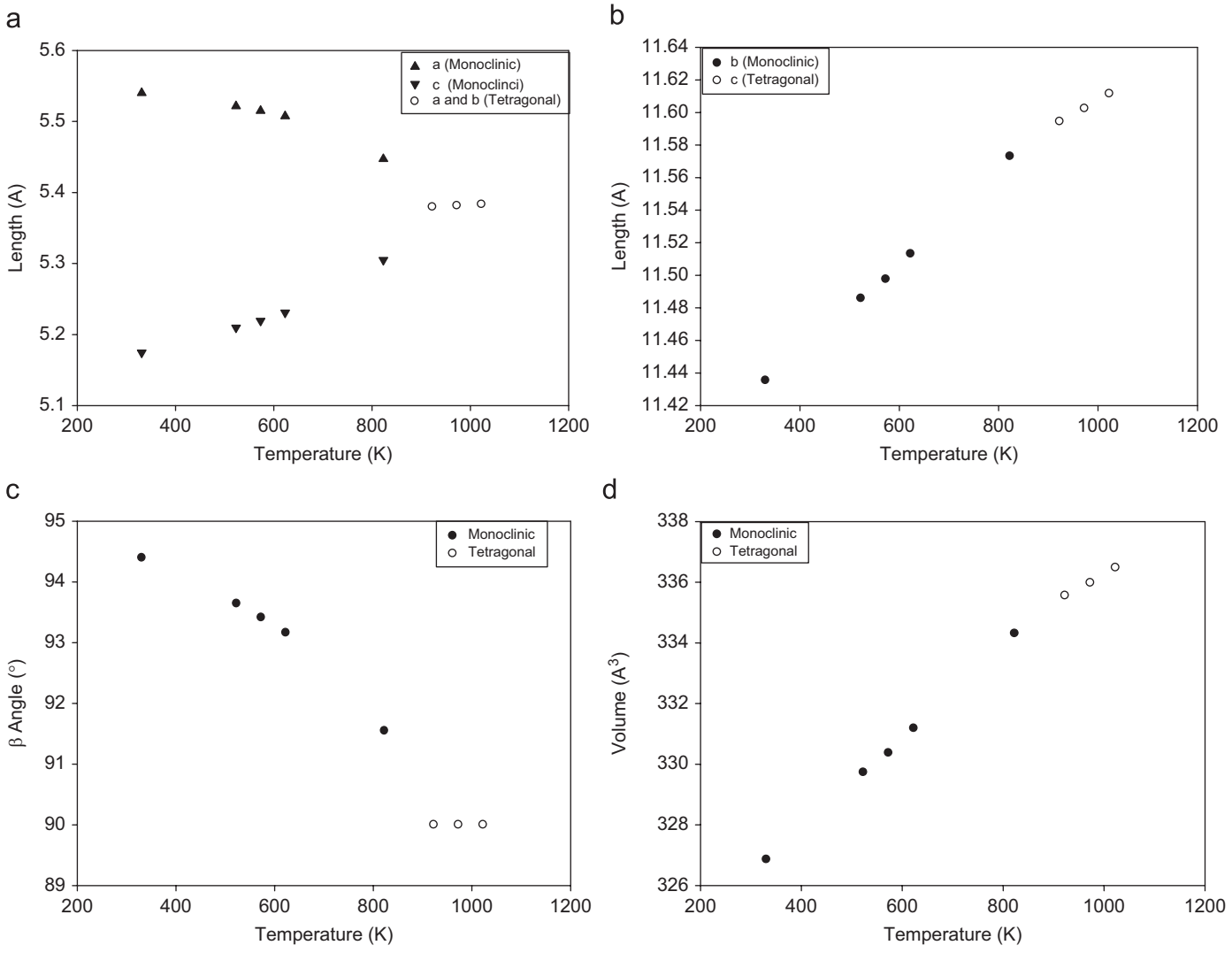

Fig. 6. Variation of (a) a and c lattice parameters, (b) b lattice parameter, (c) β angle and (d) unit cell volume with temperature for $Ce_{0.8}La_{0.2}NbO_{4+\delta}$ refined from *in-situ* high-temperature neutron diffraction.

oxidises to a $CeNbO_{4.25}$-like phase by 710 K. Once again this is consistent with weight gain TGA data reported elsewhere [11]. Additionally the TGA/DTA data also identified a two-stage process occurring at the temperature of the phase change. This can be attributed to the reduction of the material to a $CeNbO_{4.08}$-like transitional phase before the second stage tetragonal phase change seen in the HT-XRD and neutron diffraction data.

On heating the $Ce_{0.4}La_{0.6}NbO_{4+\delta}$ material (Fig. 7(b)), we see different behaviour to that of the other three phases as although it oxidises at 613 K, like the $Ce_{0.8}La_{0.2}NbO_{4+\delta}$ and $Ce_{0.6}La_{0.4}NbO_{4+\delta}$ materials, it does not fully oxidise and in fact resembles the

$CeNbO_{4.08}$ phase up to the phase change at 855K. TGA data [11] confirms this with a plateau of weight gain that if attributed solely to oxidation would lead to material of composition $Ce_{0.4}La_{0.6}NbO_{4.06}$.

Table 8
Variation of bond lengths and angles with temperature for $Ce_{0.8}La_{0.2}NbO_{4+\delta}$ as refined from *in-situ* high-temperature neutron diffraction data

T (°C)	T (K)	Ce–O1 (Å)	Nb–O1 (Å)	O1–Ce–O1 (°)	O1–Nb–O1 (°)
58	331	2.50763(5)	1.94122(5)	85.189(2)	129.005(2)
250	523	2.56430(4)	1.91251(4)	85.531(2)	130.205(1)
300	573	2.56793(5)	1.91003(4)	85.579(2)	130.081(2)
350	623	2.57223(5)	1.90741(4)	85.619(2)	129.936(2)
550	823	2.64965(9)	2.01244(8)	85.883(4)	128.833(3)
650	923	2.5176(34)	1.8448(35)	72.99(8)	106.24(10)
700	973	2.4990(32)	1.8726(34)	73.39(8)	106.45(9)
750	1023	2.49912(3)	1.87465(2)	73.423(1)	106.493(1)

Cerium bond length is for a selected Ce–O1 bond.

3.4. Guide to phase composition on heating

Given the results of the HT-XRD experiments a guide to phase composition on heating in static air was constructed and is shown in Fig. 8. To complete this diagram, HT-XRD data was collected for $CeNbO_4$ and $LaNbO_4$ and is given in Figs. 9(a) and (b), respectively. The diagram highlights two main effects; firstly that addition of lanthanum reduces the temperature of the monoclinic-to-tetragonal transition. This was explained in [16] in that the larger ionic radii of La^{3+} than Ce^{3+} (and more so Ce^{4+}) leads to weaker metal atom/oxygen bonds and hence more freedom within the oxygen polyhedra which in turn leads to a lower-transition temperature.

The second feature relates to the loss of oxygen excess upon heating with addition of lanthanum. It is clear that in the lanthanum niobate and $Ce_{0.2}La_{0.8}NbO_{4+\delta}$ there is little or no oxygen uptake on heating. This can be rationlised by considering that mixed oxidation state cerium is being replaced with fixed oxidation state lanthanum. This therefore leads to reduction in the maximum amount of oxygen excess that can be charge balanced in the structure. In air the maximum amount of oxygen

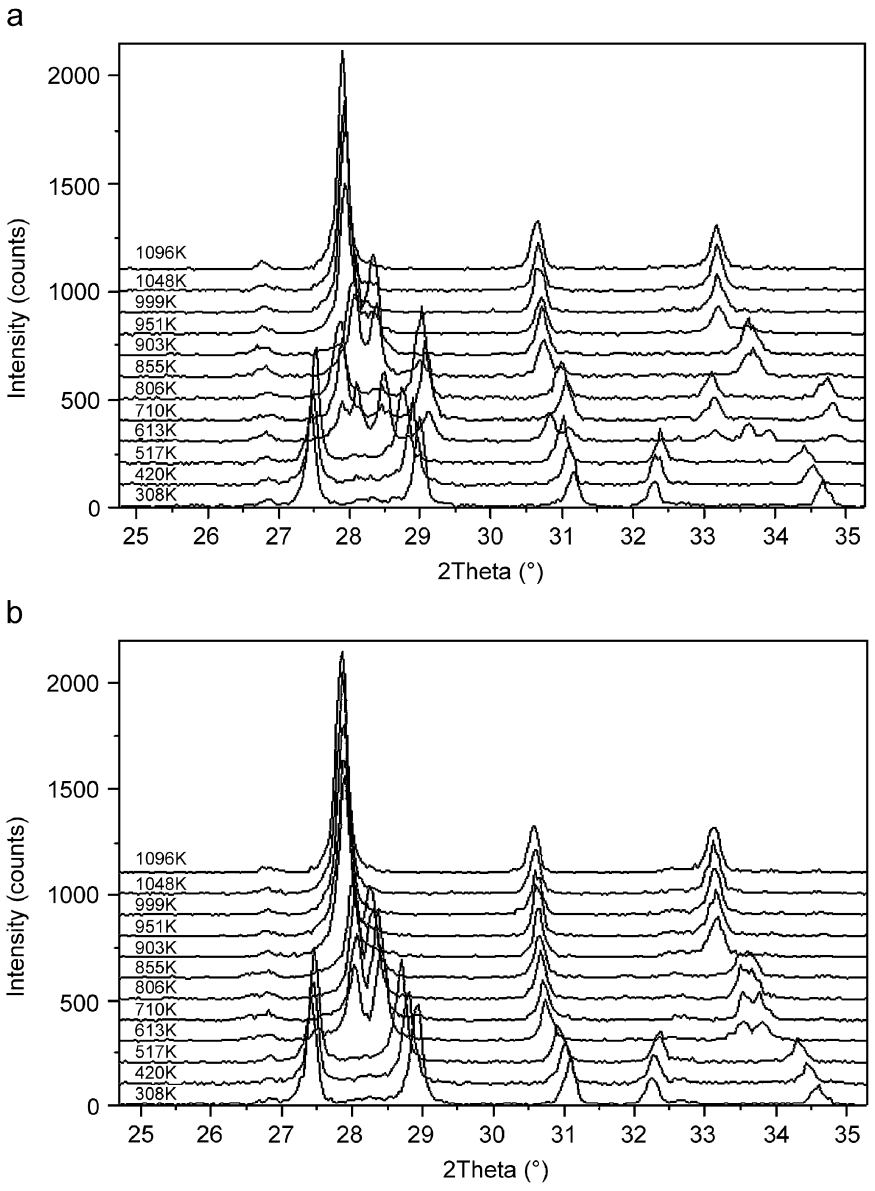

Fig. 7. High-temperature XRD data recorded on heating in static air between 25° and 35° 2θ for (a) $Ce_{0.6}La_{0.4}NbO_{4+\delta}$ and (b) $Ce_{0.4}La_{0.6}NbO_{4+\delta}$.

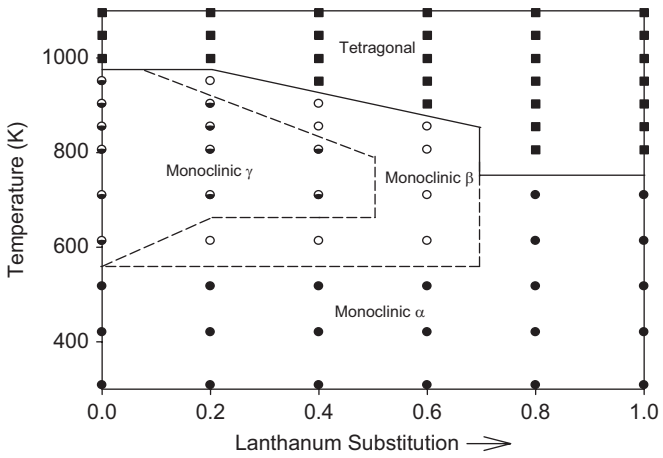

Fig. 8. Guide to phase composition for the $Ce_{1-x}La_xNbO_{4+\delta}$ series on heating in static air. Monoclinic α is analogous to the parent material, $CeNbO_4$ phase, monoclinic β with the $CeNbO_{4.08}$ phase and monoclinic γ with $CeNbO_{4.25}$. The dotted lines between the monoclinic phases indicate that these regions are guides to the predominant phase.

excess, that can be contained in the parent cerium niobate is 0.25. As oxygen has a 2− charge this corresponds to half the cerium in the structure oxidising from Ce^{3+} to Ce^{4+}. It can therefore be assumed that the maximum amount of cerium that can be oxidised in these structures in air is 50% (can be 66.6% in pure oxygen). Eq. (1) shows this oxidation mechanism for the unsubstituted cerium niobate. Eq. (2) shows the substitution mechanism of lanthanum for cerium and finally Eq. (3) shows the oxidation process of the lanthanum-substituted cerium niobates indicating the 25% reduction in oxygen interstitials per lanthanum

$$8Ce_{Ce}^{x} + 8Nb_{Ce}^{x} + 32O_{O}^{x} \xrightarrow{O_{2(g)}} 4Ce_{Ce}^{x} + 4Ce_{Ce}^{\bullet} + 8Nb_{Nb}^{x} + 32O_{O}^{x} + 2O_{i}'' \quad (1)$$

$$2La_2O_3 \xrightarrow{8CeNbO_4} 4La_{Ce}^{x} + 6O_{O}^{x} \quad (2)$$

$$4Ce_{Ce}^{x} + 4La_{Ce}^{x} + 8Nb_{Ce}^{x} + 32O_{O}^{x} \xrightarrow{\frac{1}{2}O_{2(g)}} 2Ce_{Ce}^{x} + 2Ce_{Ce}^{\bullet} + 4La_{Ce}^{x} + 8Nb_{Nb}^{x} + 32O_{O}^{x} + O_{i}'' \quad (3)$$

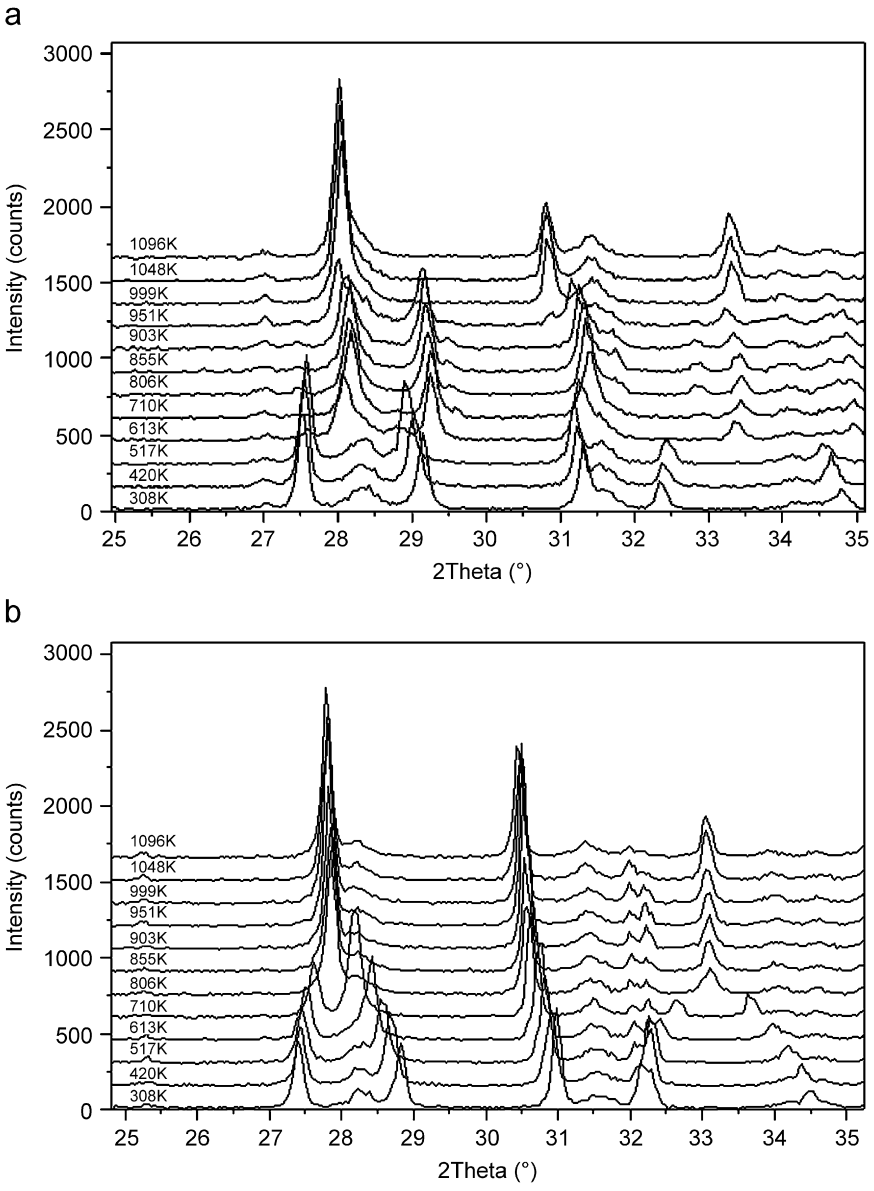

Fig. 9. High-temperature XRD data recorded on heating in static air between 25° and 35° for (a) $CeNbO_{4+\delta}$ and (b) $LaNbO_4$.

If this regime is correct then this gives the maximum amount of oxygen excess for the other members of the series as, $Ce_{0.8}La_{0.8}NbO_{4.2}$, $Ce_{0.6}La_{0.4}NbO_{4.15}$, $Ce_{0.4}La_{0.6}NbO_{4.1}$ and $Ce_{0.2}La_{0.8}NbO_{4.05}$. These values are close to those obtained experimentally using TGA analysis and therefore support this assumption. In terms of Fig. 8, to obtain these calculated values a mixture of hyperstoichiometric phases would need to be present or that the materials referred to as $\delta = 0$, 0.08 and 0.25 are not line phases but exist over a range of stoichiometries. It is of course possible that both situations exist in this complex system. This therefore indicates that although the diagram is accurate for the monoclinic-to-tetragonal phase change, the oxidation state changes for the monoclinic phases, corresponding to structural changes, are intended primarily as a guide to the predominant phase (hence dotted lines) under the described heating conditions and is hence presented as a guide to phase composition rather than a phase diagram. This 50% cerium oxidation method would therefore explain why the $Ce_{0.4}La_{0.6}NbO_{4+\delta}$ phase does not show any of the $CeNbO_{4.25}$-like phase in the XRD pattern (termed monoclinic γ in the composition diagram) but a large region of the $CeNbO_{4.08}$-like phase (termed monoclinic β in the composition diagram).

4. Conclusion

The neutron diffraction data show that with increasing amounts of lanthanum substitution there is an associated reduction in the temperature of the monoclinic-to-tetragonal phase transition and suggests a decrease in the amount of excess oxygen. The high-temperature X-ray data corroborates the findings of the neutron experiments and also suggests the formation of an intermediate phase during the phase transition for the $x = 0.8$ and 0.6 phases which appears to be similar to the $CeNbO_{4.08}$ phase seen in the parent material. From this data a guide to phase composition was constructed and shows that on addition of lanthanum the maximum levels of oxygen excess on heating decrease.

Acknowledgments

The authors would like to thank the CCLRC for funding this work (RB520261) and Dr. Richard Ibberson, HRPD instrument scientist, for his contribution in carrying out the neutron experiments. Mr. Richard Sweeney at Imperial College was also invaluable for helping with the high-temperature XRD data. We would also like to thank the EPSRC for the award of a doctoral training account studentship (RJP).

References

[1] A. Lashtabeg, S.J. Skinner, J. Mater. Chem. 16 (2006) 3161–3170.
[2] S.C. Singhal, K. Kendall, High Temperature Solid Oxide Fuel Cells: Fundamentals, Design and Applications, Elsevier, Amsterdam, 2003.
[3] C.N. Munnings, S.J. Skinner, G. Amow, P.S. Whitfield, I.J. Davidson, Solid State Ionics 176 (2005) 1895–1901.
[4] M.J. Escudero, A. Aguadero, J.A. Alonso, L. Daza, J. Electroanal. Chem. 611 (2007) 107–116.
[5] G.J. McCarthy, Acta Crystallogr. B 27 (1971) 2285–2286.
[6] J.G. Thompson, R.L. Withers, F.J. Brink, J. Solid State Chem. 143 (1999) 122–131.
[7] S.J. Skinner, I.J.E. Brooks, C.N. Munnings, Acta Crystallogr. C 60 (2004) I37–I39.
[8] E.V. Tsipis, C.N. Munnings, V.V. Kharton, S.J. Skinner, J.R. Frade, Solid State Ionics 177 (2006) 1015–1020.
[9] R.J. Packer, E.V. Tsipis, C.N. Munnings, V.V. Kharton, S.J. Skinner, J.R. Frade, Solid State Ionics 177 (2006) 2059–2064.
[10] L. Jian, C.M. Wayman, J. Am. Ceram. Soc. 80 (1997) 803–806.
[11] R.J. Packer, S.J. Skinner, A.A. Yaremchenko, E.V. Tsipis, V.V. Kharton, M.V. Patrakeev, J. Bahteeva, J. Mater. Chem. 16 (2006) 3503–3511.
[12] A.C. Larson, R.B.V. Dreele, Los Alamos National Laboratory Report LAUR (2000) 86–748.
[13] B.H. Toby, J. Appl. Cryst. 34 (2001) 210–213.
[14] A. Santoro, M. Marezio, R.S. Roth, D. Minor, J. Solid State Chem. 35 (1980) 167–175.
[15] M. Machida, J. Kido, T. Kobayashi, S. Fukui, N. Koyano, Y. Suemune., Kyoto University, Research Reactor Institute: Annual Report 28 (1995) 25–32.
[16] K.A. Gingerich, H.E. Blair, Adv. X-ray Anal. 7 (1963) 22–30.
[17] S.J. Skinner, Y. Kang, Solid State Sci. 5 (2003) 1475–1479.